
Stability Analysis of Continuous Welded Rails Using New Non-Destructive Technology

Ralph Zhang, Helen Wu, and Chunhui Yang

School of Computing, Engineering and Mathematics, Western Sydney University, Penrith, Locked bag 1797, NSW 2751, Australia

*Corresponding author's email: wei.zhnag@transport.nsw.gov.au

Peer review history

Manuscript submitted: 23 April 2019

Review process completed: 19 August 2019

Manuscript finally accepted: 19 August 2019

Handling Editor: Professor Chin Leo

Abstract: For the safety management of CWR track, the primary is to obtain the accurate neutral temperature of the CWR track (i.e. the value and distribution of the longitudinal stress within the rail). In the recent decade, some newly developed technologies have been utilised for the non-destructive neutral temperature measurement. The Magnetic Barkhausen Noise (MBN) technology is one of them. Within this paper, a series of in-field verifications and data comparison results which are obtained on Australian heavy haul mainline tracks are presented. These results have shown that this MBN measurement system can provide high accurate and reliable neutral temperature results. By using this effective measurement tool, the

neutral temperature on several critical rail lines has been measured. Among these lines, the track structures and conditions are in high diversity. To study the details of the longitudinal stress distribution within the variable CWR tracks, the non-linear finite element analysis modelling is utilised to simulate the track conditions, ambient temperature changing and structural features. The major outcomes from this study including: Firstly, the fastening system and sleeper spacing for a specified CWR track module can significantly impact to its stability. Secondly, for the CWR tracks which are installed on the sharp curves and steep slope, the neutral temperature (longitudinal stress) is not evenly distributed within the CWR module. Thirdly, bending stress in the rails that installed on the sharp curves can influence the thermal stress distribution in the longitudinal direction and it seems it is sensitive with the radius of the curve.

Keywords: High-rise buildings, transfer plate, finite elements, two-stage analysis.

1. Introduction

Obtaining the longitudinal stress (also known as “Neutral temperature” of CWR track in railway industry (Kerr, 2003)) by the non-destructive method is the “Holy Grail” of the continuous welded rails (CWR) track maintenance (Moller, Radmann & Zhang, 2009). Using the non-destructive method to measure the longitudinal thermal stress in CWR tracks is the major important effort direction for railway track engineers and researchers for decades. In the recent years, especially in the last decade, some relative “matured” technologies have been applied for the non-destructive measurement of the longitudinal stresses in the CWR track. The Magnetic Barkhausen Noise is one of them and it has been tested and improved for more than two decades (Wegner, 2004 and Wegner, 2007). Using the finite element method to study the stability of CWR track is started since the beginning of this century (Zhang & Wu, 2006 & Wang, 2015). The utilisation of finite element software ANSYS for this study also can go back to that time (Yang & Gu, 2006).

The Sydney-Broken Hill railway line is now part of the transcontinental railway from Sydney to Perth, which plays very important roles in Australian railway network. The railway line started to connect Sydney (the biggest chief-city on the East Coast of Australia) with the inner of the Australian continental since 1855, until an isolated section of standard gauge line was opened from Menindee to Broken Hill in 1919. In 1969 the last section of the Broken Hill line's gauge was standardised, completing the Sydney - Perth standard gauge link. Originally, this rail line was designed and constructed in the early 20 century with a lower standards and price. On this line, many low strengthen track modules are existed, such as lower rail type (53kg/m rail), low strengthen timber sleepers, sharp curves, steep gradient, etc. To maintenance the stability of the CWR tracks in the very harsh environments passing central desert and facing extremely hot weather in summer time are a great challenge to the permanent of way (Kish, 2009).

To keep the stability of the CWR tracks for the growing freight revenue, the owner of this line found they are facing great challenges from high cost, shortage of man-power, hazard environment conditions and without effective and reliable

inspection equipment. To solve these problems, the RailScan™ system (the equipment based on the MBN technology) was applied as one of the non-destructive CWR neutral temperature testing systems for a feasibility study (Wegner, Hofmann, Radmann, Zhang & Dubbins, 2011). The results represented in this paper are based on two in-field measurements in 2008 and 2009, in Ivanhoe, Menindee, Kinalung, and Broken Hill areas, NSW, respectively.

2. Magnetic Barkhausen Noise Technology

The magnetic Barkhausen noise technology was equipped within a smartly designed machine - RailScan system to carry out the measurement of longitudinal stress distribution in the CWR tracks. Based on the micro-magnetic theory, every part of ferromagnetic materials contributes to the uniform magnetisation. The internal magnetisation is not uniform down to a microscopic scale. Many magnetic domains are magnetised in different directions. The magnetisation inside each domain is made up of many microstructural zones which are lined up by the action of their exchange forces. The schematic drawing of the domain structure is shown in Figure 1.

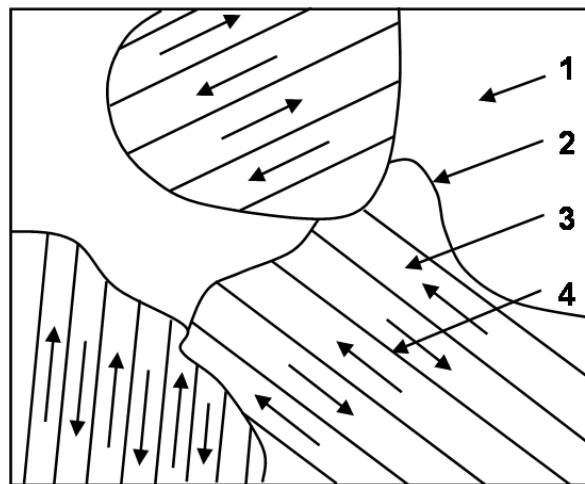


Figure 1: Domain structure of ferromagnetic substances (1-crystallite, 2-grain boundary, 3-Weiss's domain, and 4-Bloch-wall), Chikazumi (1964).

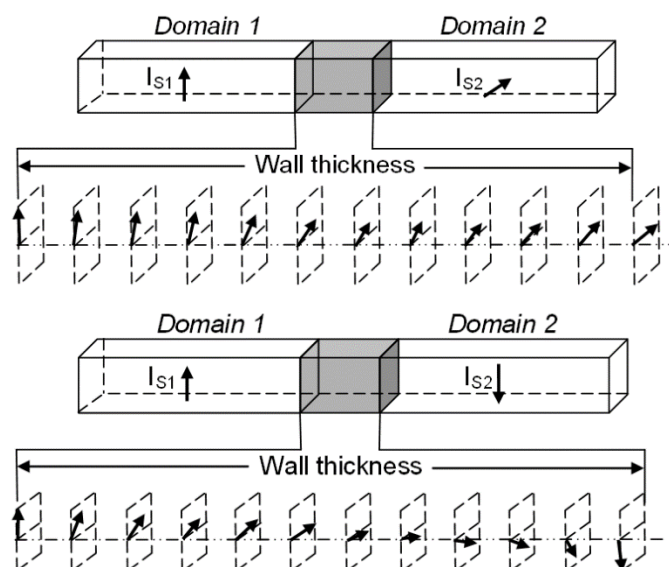


Figure 2: Change of the magnetisation vector in Bloch-walls. 90°-Bloch-wall (BW1-upper figure) and 180°-Bloch-walls (BW2-lower figure, Chikazumi (1964))

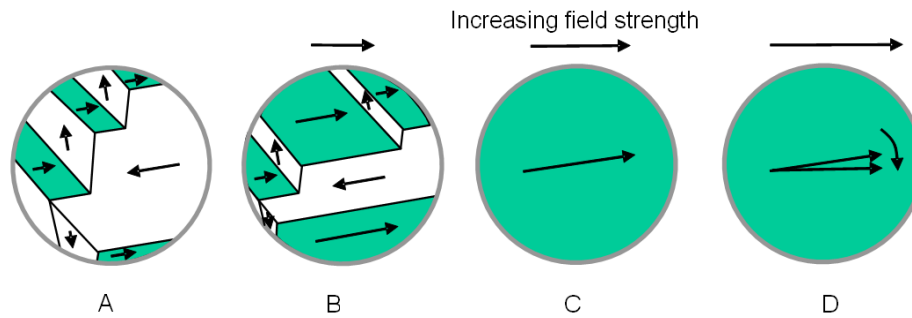


Figure 3: Magnetisation in a [110] direction of Si-Fe: A: domain structure, B-D: orientation process under the action of an increasing magnetic field, Chikazumi (1964).

The crystallites are limited by grain boundaries while the magnetic domains are limited by the Bloch-walls. The domain structure was first predicted by Weiss in 1907 and experimentally verified by Barkhausen in 1919. In 1932, Bloch described that the boundary between the domains is not sharp on an atomic scale but is spread over a certain thickness wherein the direction of spins changes gradually (Chikazumi, 1964). The effect of the existence of such Bloch-walls is shown in Figure 2. Two kinds of Bloch-walls are defined in this figure ---- the 90°- (BW1) and the 180°-Bloch-wall (BW2).

If a magnetic field is applied, the two kinds of domains whose magnetisation directions are closest to the field direction increase their volumes and finally cover the whole domain (Figures 3 B-D). If the field is increased further, the magnetisations in each domain rotate from their easy directions toward the field direction, and finally the saturation magnetisation can be reached (Figure 3d). This process is typical as one important feature of ferromagnetic substances. They exhibit a fairly complex change in magnetisation upon the application of a magnetic field.

This behaviour can be described by a magnetisation curve possessing three distinct regions (Figure 4). Starting from a demagnetised state, the magnetisation increases (broken curve) and finally reaches the saturation magnetisation. In the region “I” the process of magnetisation is almost reversible. That is, the magnetisation comes back to zero upon removal of the field. The domain walls move reversibly and will return to their original position if the field is removed. Beyond this region the processes of magnetisation are no longer reversible. In the low-field region “II” the domain wall movement occurs irreversibly as walls overcome barriers presented by pinning centres in the microstructure. In the highest field region “III” only little domain wall motion occurs and further magnetisation is predominantly due to rotation of the magnetisation vector within individual domains.

In the domain of irreversible wall movement the hysteresis loop has the shape of a stair and Barkhausen jumps occur in the form of micro- eddy currents (enlarged increments on the left side of Figure 4)

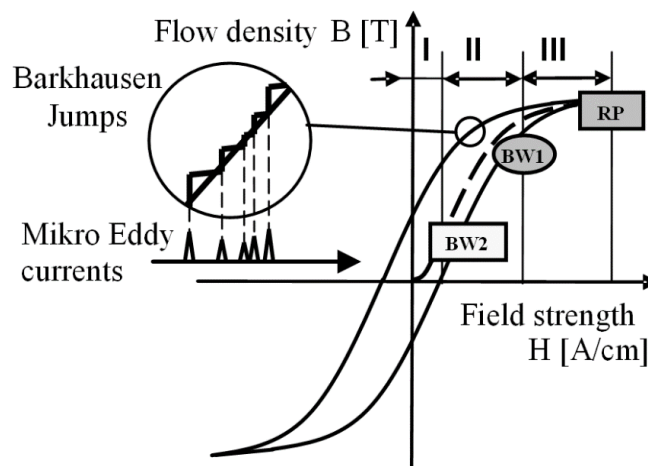


Figure 4: Hysteresis loop: Magnetisation regions I, II and III starting from a demagnetised state and field dependent magnetisation processes by Bloch-wall types BW1 and BW2.

It is essential for further understanding to know the interactions of the different Bloch-walls during the magnetisation. Bloch-walls of the first kind (BW1) are walls which separate magnetic domains in which the residual stresses do not vanish in adjoining domains. In iron all (100)-90° BWs are of this type. Bloch-walls of the second kind (BW2) produce only residual stresses within themselves. In iron all 180° Bloch-walls and the (110)-90° walls are of this type. BW2s separate areas with the same magnetostrictive behaviour and consequently no elastic energy will be changed during their movements. Therefore, BW2s do not interact with macro stresses RS1 and micro stresses RS2. Beside BW1 all rotation processes (RP) are stress sensitive.

BW1, BW2 and RP exist at different magnetic field strengths to the magnetisation process (Figure 4). Following previous work, in polycrystalline ferrous materials BW2 contribute to the magnetisation in a dominant way around the coercively field strength H_c . Outside of this field region BW1 becomes more and more dominant. If magnetisation becomes saturated, BW density decrease and finally remagnetisation processes take place contributed by RPs (Figure 3). Because of these micromagnetic interactions with the microstructures, all the parameters can be recorded with one set of micromagnetic quantities. Hereby stresses are measured by values mainly determined by BW1.

At the microstructural level, the magnetisation process consists of many small discontinuous flux changes, which correspond to the irreversible movement and flopping of Bloch-walls and domains. During this process, micro eddy currents are induced in the domain (Figure 4), enlarged increments of hysteresis loop. These so-called Barkhausen jumps can be measured by using an appropriate detector. Along the hysteresis loop, the MBN shows two maxima around the coercive field strength H_c . The effective value of MBN is generally recognised as a measure for quantitative non-destructive evaluations. It contains the generated pulses and has a noise-like spectrum.

The stress sensitivity of BW1 and RP can be used to measure the longitudinal stress in the rail. In any load stresses applied, the permeability for the applied magnetic field changes. Tension leads to an increase of the permeability. The higher the longitudinal stress, the higher the increase of permeability. The rail becomes more and more magnetisable then.

When compression stress is applied, the rail becomes magnetically hard with increasing compression. The permeability for the magnetic field decreases. This Villari-effect is measurable by analysing Magnetic Barkhausen Noise (MBN) signals. The MBN contains the eddy currents of the stress sensitive parameters BW1 and RP and depends significantly of the longitudinal stress in the rail. Tension increases the amplitude of the MBN, whilst compression leads to decreases. The higher the longitudinal stress, the higher the signal amplitude of the MBN. MBN has the sensitivity with stress conditions in metal materials, which was found by physicists since last century, and it can be equipped with different types of devices to measure the stress condition in CWR rails for decades.

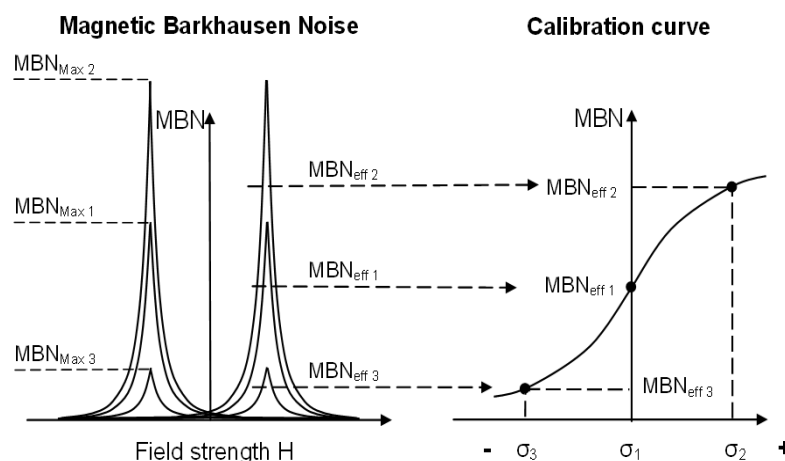


Figure 5: Stress dependence of the MBN used for reconstructing a MBN-stress relationship

3. Measurement Device and Its Operation

The RailScan® system was designed to measure the stress distribution and the Neutral Temperature of continuously welded rails (CWR). The device operates by means of non-contact gauging using the magneto-elastic principle and allows

fast measurement and documentation of the actual Neutral Temperature of rails. The longitudinal stress and the Neutral Temperature are determined by measuring characteristic magnetic values.

The rail is magnetised by applying an alternating magnetic field. Interactions of the magnetic field with the magnetic microstructure are orientation dependant and can be measured with an appropriate probe. The measured signals contain the pulses generated in the rail and have noise-like spectrums. The amplitude of this Magnetic Barkhausen Noise (MBN) depends significantly on the longitudinal stress in the rail. Tension increases the amplitude of the MBN, whilst compression leads to decreases. The higher the longitudinal stress, the higher the signal amplitude.



Figure 6: TRACKSAFE RELEASE (the updated version of RailScan® system) unit

The RailScan® system consists of a manually operated railcar, a central unit, and a pair of probe (Figure 6). The central unit contains the computer-operated measuring electronics. A separate battery provides the power supply for the equipment. The probe consists of two yokes that are pressed around the rail-head with the help of a Bowden wire and springs. The replaceable probe is geometrically adapted to the rail type. The rail temperature is measured with an integral infrared thermometer.

Before performing the measurement the rail was marked. The measurement was made after positioning the device above each mark in turn. The rail was energised by a magnetic field in the acoustic frequency range, and the level of the Magnetic Barkhausen Noise at the surface of the energised region was measured. One measurement series consisted of 50 marked points.

Evaluation was performed automatically after the measurement. The measurement result can be stored and visualised on a PC via data transfer. Data can be read and processed by using Microsoft Office

4. Calibration

Before the RailScan measurements, for each type of rail, the RailScan device must be calibrated in the laboratory using at least three calibration rails, which are the same type and under similar condition with the rails were measured on the track. The calibration rail samples were gauged by strain gauges. The calibration work was carried out by hydraulic rail tensor, and the data are analysed by Weibull factor. On this occasion, measurements of the MBN are taken for different longitudinal stresses and used for obtaining a calibration curve of the MBN as a function of longitudinal stress. The calibration curve of AIS 107LB rail (which is a type of widely used rail on Australian railway network) from these three rail samples is shown in Figure 7. The calibration curve was be used as the base line and collation form, and it worked together with the in-field testing results to determine the neutral temperature of a specified rail track section. Hence, this procedure is a very important section of the measurement. Its results can greatly influence the accuracy of the whole work.

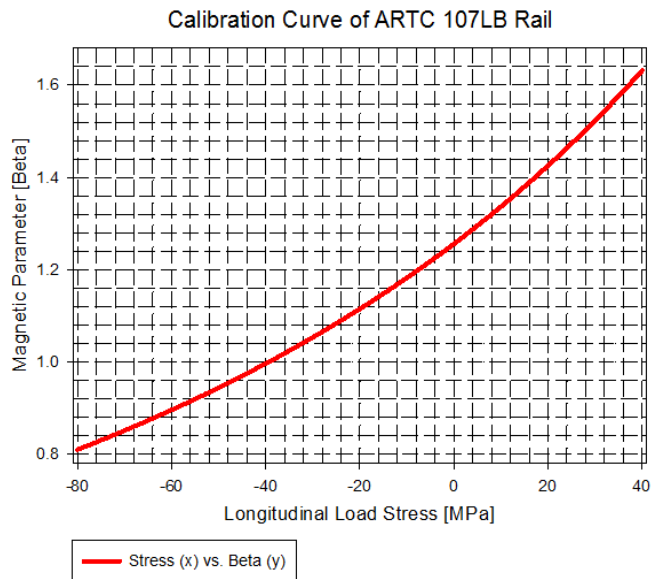


Figure 7: Calibration curve of AIS 107LB plain carbon rail

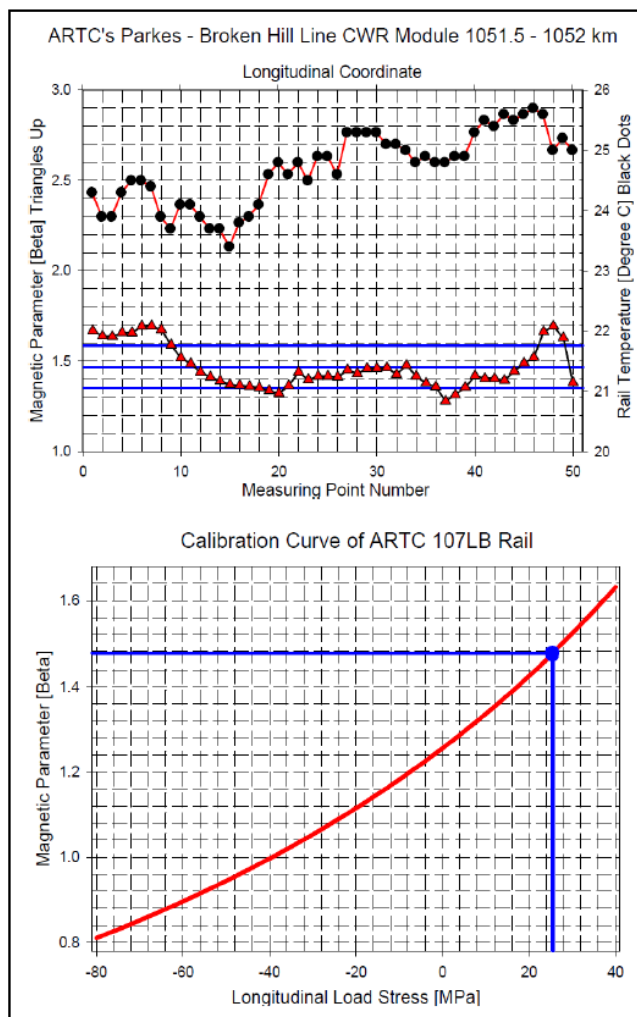


Figure 8: Above: Stress sensitive parameter and rail temperature, plotted vs. longitudinal coordinate. Bottom: Longitudinal load stress determined by means of the rail specific calibration curve.

5. Data Analysis

After completing the measurements the raw data were downloaded to a laptop for further evaluation. The final results were obtained by evaluating and plotting the measured values of the magnetic parameter and rail temperature vs. the longitudinal coordinate and measuring point number and further by depicting the load stress determined by means of the averaged magnetic parameters and calibration curve. The final results were obtained by evaluating and plotting the measured values of the magnetic parameter and rail temperature vs. the longitudinal coordinate and measuring point number and further by depicting the load stress determined by means of the averaged magnetic parameters and calibration curve. As an example, the results and relative calibration information of the CWR module at 1051.5 km - 1052 km are shown as in Figure 8.

The neutral temperature can be calculated by means of the following equation:

$$T_N = \frac{\sigma_L}{E \times \alpha} + T_{Rail}$$

Where:

T_N - The neutral temperature before de-stressing;

T_{rail} - Rail temperature when doing the RailScan measurement;

σ_L - The longitudinal stress in the CWR rail;

α - Thermal coefficient of rail, using 11.5×10^{-6} (m/°C);

E - Elastic modulus, using 2.07×10^5 MPa.

6. Comparison and Confirmation of RailScan Results

Since the year 2006, around 300-km CWR track measurements were conducted on Australian heavy haul operated railway lines. The in-field measurement results were compared with some widely acknowledged method/equipment to confirm the accuracy and reliability of the RailScan system. The results are represented in this paper are from two in-field measurements in 2008 and 2009 on Parkes – Broken Hill Line, respectively. One is in Ivanhoe, and the other is in Menindee.

A series of data comparisons were performed on the data from the in-field testing with the results from VERSE System (which is a commercial product of VORTOK International) and A-Frame (which is a simplified VERSE system).

Considering the Verse system is significantly limited by the operational rail temperature (As the method only can be applied to tracks in tension, the ambient temperature must be lower than the true T_N) and the characteristics of track modules (do not has very accurate track modules for the variable track condition of “timber sleeper assembled by low toe load dog spike” as an input for neutral temperature calculation which combined with the directly in-field measurement results), the results obtained by using the two systems were measured with similar or significant different ambient conditions, hence, the comparisons were conducted separately.

a. Different time but closer rail temperature

Because when VERSE performs its neutral temperature measurement, the track must be un-clipped. Usually, the air temperature when performing the un-clipping works is different to the neutral temperature, and the original neutral temperature can be changed by this way. Hence, the RailScan measurements were carried out before the VERSE system. The results of RailScan and VERSE measured at the closer rail/ambient temperature conditions ($\pm 5^\circ\text{C}$) are represented in Figure 9.

For the situation of the two methods carried out the measurement at different time but closer rail temperature, the results are quite close. The average difference between these two methods is 1.47°C , which is very close. In addition, for these modules the RailScan measurement can be early or later for the Verse measurement and the time gaps are also changed from one day to 3 weeks.

Theoretically, it can be explained as the “change” of the original neutral temperature that caused by the Verse measurement was “destressed” by the railway traffic and relatively lower track frame stiffness (because of the lower toe load of the fasteners).

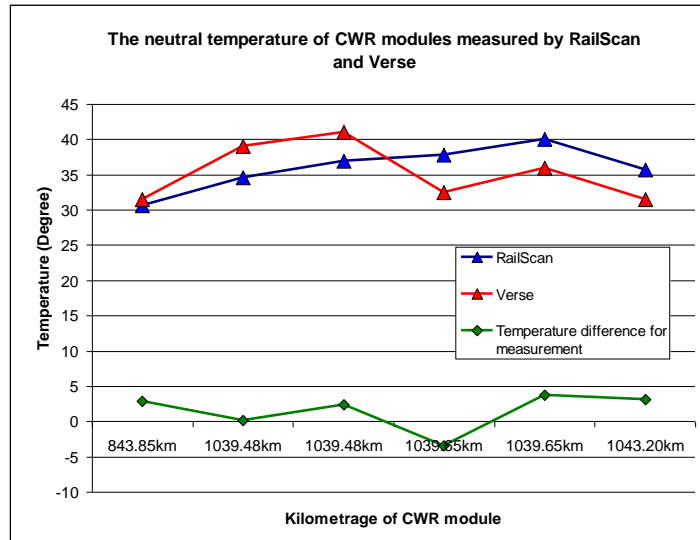


Figure 9: The neutral temperatures of CWR modules measured by RailScan and VERSE

b. Different time with significant different rail temperature

As shown in Figure 10, the results from RailScan and VERSE are significantly different. Because of the VERSE system can only operate in a narrow rail temperature range, therefore, for these modules the rail temperature measured using RailScan and VERSE has an average of 16.7 °C. In addition, the structural strength of the CWR track on the Broken-Hill line was found also relatively low. For example, the track was installed with timber sleepers, reused steel sleepers and dog-spike fasteners, with the extreme high temperature conditions, the creep of CWR track could happened. This creep can be explained as the major reason that caused the 11.5 °C of average neutral temperature result between RailScan and VERSE measurement with an averagely rail temperature difference of 16.7 °C.

Studying the CWR resistant load from the fasteners, the basic concept of fastener design is the longitudinal resistance from the fastener must higher than the ballast resistance on the sleeper, hence, to ensure the rail will not creep on the top surface of the rail seat of sleeper. Therefore, the sleeper, fasteners, and ballast can work together as a frame to provide adequate resistant force for the stability of CWR track.

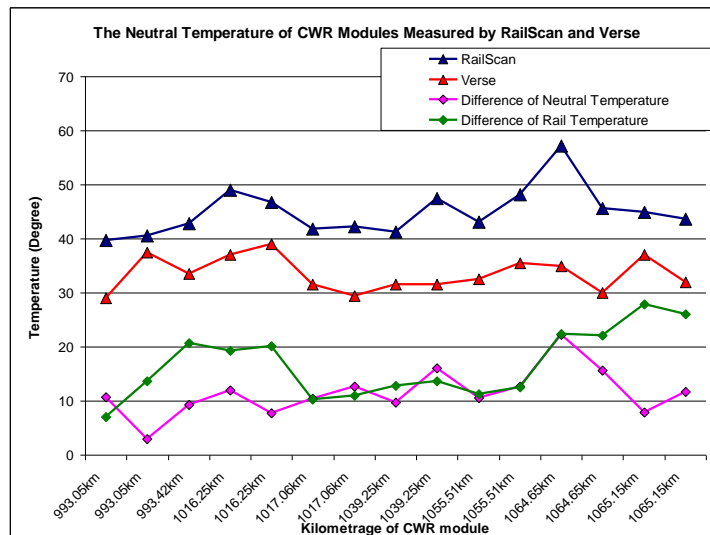


Figure 10: The neutral temperature of CWR modules measured by RailScan and Verse

For a specified CWR track module (1064.65 km):

- With dog-spike fastener, the average toe load using 6 kN (very tightly connected with rail) to very low (for the spike pull-out condition), practically, for the CWR track design, the recommended value by Chinese Railway is 1.25 kN/spike.
- With Trak-Lok fastener, the average toe load using 6 kN/fastener (the usage times surpass its fatigue limitation).

- With Pandrol PR 300 fastener, the average toe load using 6.2 kN/fastener.

For the anchors, they were installed in the style of one in forth as shown in Figure 11. Regarding to the resistance load that provided by the one anchor on one direction, assuming its capability is 15 kN in good installation condition.

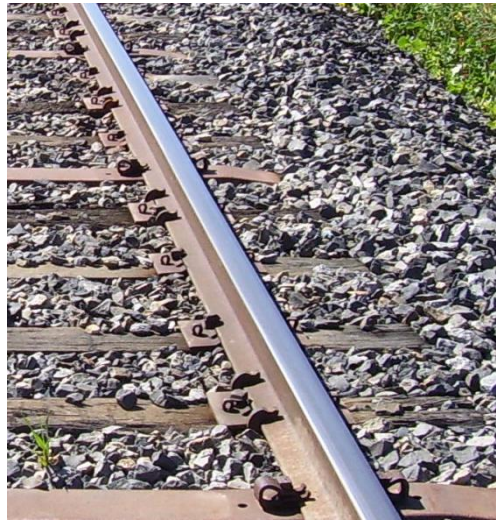


Figure 11: The anchors installed of the CWR track

Table 1: Detailed of the sleeper of the module of 1064.65 km

Frequency number	Sleeper/Fastener type	Frequency number	Sleeper/Fastener type
1	Timber/dog-spike	26	Timber/dog-spike
2	Steel/Trak-Lok	27	Steel/Trak-Lok
3	Timber/Pandrol PR 300	28	Timber/dog-spike
4	Timber/dog-spike	29	Timber/dog-spike
5	Timber/dog-spike	30	Timber/dog-spike
6	Steel/Trak-Lok	31	Timber/dog-spike
7	Timber/dog-spike	32	Timber/dog-spike
8	Timber/Pandrol PR 300	33	Timber/dog-spike
9	Timber/dog-spike	34	Steel/Trak-Lok
10	Timber/dog-spike	35	Timber/dog-spike
11	Timber/dog-spike	36	Timber/dog-spike
12	Timber/dog-spike	37	Timber/Pandrol PR 300
13	Timber/dog-spike	38	Timber/dog-spike
14	Steel/Trak-Lok	39	Timber/dog-spike
15	Timber/dog-spike	40	Timber/dog-spike
16	Timber/dog-spike	41	Timber/dog-spike
17	Timber/dog-spike	42	Timber/dog-spike
18	Timber/dog-spike	43	Timber/dog-spike
19	Timber/dog-spike	44	Timber/dog-spike
20	Timber/dog-spike	45	Steel/Trak-Lok
21	Timber/dog-spike	46	Timber/dog-spike
22	Timber/dog-spike	47	Timber/dog-spike
23	Timber/dog-spike	48	Timber/dog-spike
24	Timber/dog-spike	49	Timber/dog-spike
25	Timber/dog-spike	50	Timber/dog-spike

For the longitudinal axial resistance of timber sleeper, according to the study carried out by Dr. Arnold Kerr in USA (Kerr, 2003), the maximum value is around 9 kN for timber sleeper with 600 mm spacing. In addition, the friction coefficient factor between rail and steel fastener is: 0.2. Using the sleeper data of the module of 1064.65 km, as shown in Table 1, as input data and we obtained the average fastener resistance on each sleeper against one rail is:

$$\{[(\text{Dog-spike: } 42) \times 1.25 + (\text{Trak-lok: } 6) \times 6 + (\text{Pandrol PR: } 2) \times 6.2] \times 4 \times 0.2 + (\text{Steel Anchor one direction: } 11) \times 15 \times 2\} / 50 = [(52.5 + 36 + 12.4) \times 4 \times 0.2 + 165 \times 2] / 50 = 8.2 \text{ kN}$$

The 8.2-kN average resistance load is significantly lower than the requirement of per sleeper ballast resistance which is 9.5 kN for timber sleepers with 600 mm spacing. That means the long rail can creep longitudinally along the rail seat of sleeper, when the rail temperature is different with the neutral temperature.

The above phenomena were confirmed by many in-field results, for example, the results of the CWR module 1065 km – 1065.5 km down rail at Kinalung. The neutral temperature distribution within the CWR module of 1065 km – 1065.5 km (Down rail) was measured twice on 11th and 12th of August, 2009 at different rail temperature. Compare their results in Figure 12 by plotting the result in one figure, it can be found that, the neutral temperature results are different, and the rail temperature on 11th August is significantly higher than that on 12th August. The difference of rail temperature is almost constant and generally the trade of the difference of neutral temperature is also similar. Studying their average values, the average difference for rail temperature is about 6 °C and the average difference of neutral temperature is 5.7 °C. It is very clear that the long rail can creep longitudinally along the rail seat of the sleepers, when the rail temperature is different than the neutral temperature

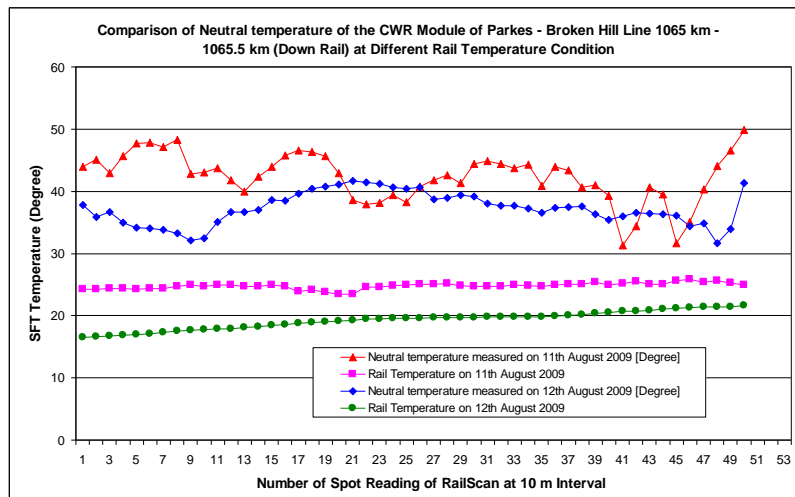


Figure 12: Comparison of neutral temperature of the CWR module of Parkes – Broken Hill Line 1065 km – 1065.5 km (Down rail) at different rail temperature conditions

a. Further study on steep slope CWR modules

The RailScan results can present the neutral temperature changes that caused by some special track structures, such as sharp curve, steep slope, etc. For example, for the CWR module of 1051.5 km – 1052 km, it has a steep slope with the falling is 1:152 (as shown in Figure 13).

The neutral temperatures, obtained from RailScan for the up rail and down rail and diagram of slope, are overlap-plotted in Figure 14. From these figures it can be found that from the start point of steep slope the neutral temperature is going to decrease and reach the minimum results at the location around the bottom of the steep slope. Hence, for the CWR module like this, the critical neutral temperature is the lowest result at the bottom at the slope.

a. Further study on sharp curves

To facilitate the analysis, details of some sharp curve CWR track modules such as the actual radius, super-elevation, start and end kilometrage of transition curve and circular curve were obtained from a database. A curve module and the β factor obtained from Rail Scan at the 50 points are plotted in Figure 15. This module was measured when it was just finish the de-stressing. The kilometrage of the CWR module is 319.630km - 319.911km (North Coast Line), which is located between two steel girder bridges (one of the bridge on the transition curve section). Some findings from the comparison of Rail Scan results and designed destressing results are presented as following:



Figure 13: CWR module of 1051.5 km – 1052 km with a steep slope of falling is 1 in 152

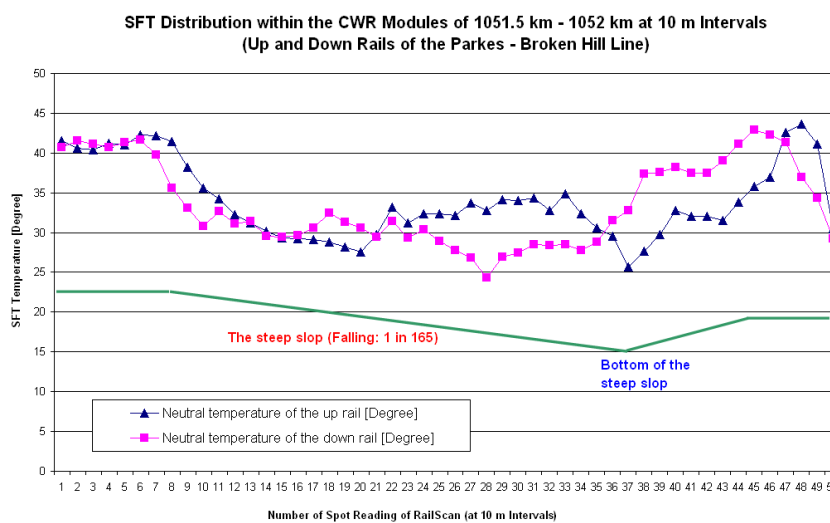


Figure 14: Neutral temperature distribution within the CWR module of 1051.5 km 1052 km (Up and down rail)

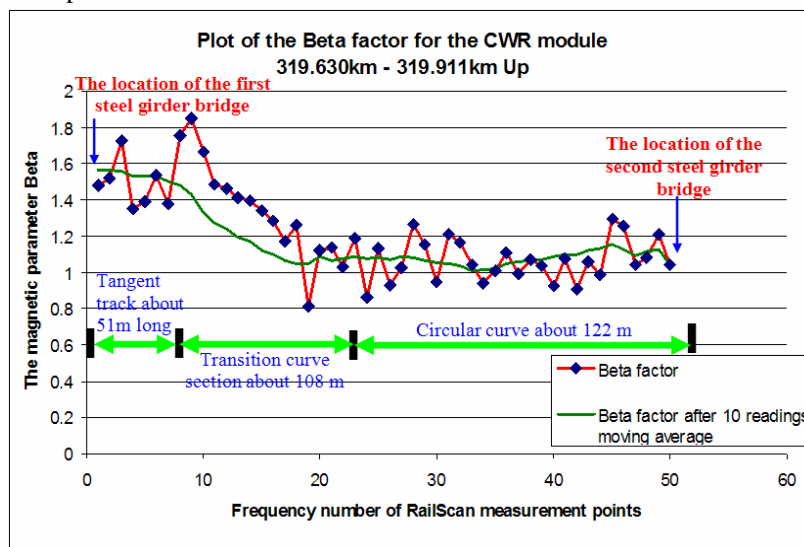


Figure 15: Plot of the factor that obtained from RailScan at the 50 points for a curve module

From Figure 15 and other sharp-curved CWR modules, a significant phenomenon is that the magnetic parameter β is not evenly distributed along the whole curve from transition curve to circular curve. For the module 319.630 km - 319.911 km, it is a combination of about 51 m tangent track, 108 m transition curve, and 122 m circular curve, for the average of their β values, it is 1.5456, 1.24606, and 1.075795, respectively. Combined with their rail temperature, the neutral temperatures are: $T_N = 46.96$ °C for tangent section, $T_N = 34.5$ °C for transition curve, and $T_N = 21.54$ °C for circular

curve. It means that in a sharp curve module, the real neutral temperature at tangent track and transition curve is dramatically higher than circular curve. Based on the knowledge of structural mechanic it can be explained as on the sharp curves the longitudinal thermal stress can be deducted by the bending stress from the sharp curvature bending moment. This phenomenon also happened with every curve modules and influenced by the radius of the curve.

7. Numerical Study of Rail Tracks

To study the details of the longitudinal stress distribution within the variable CWR tracks, the non-linear finite element analysis modelling is utilised to simulate the track conditions, ambient temperature changing and structural features.

a. Finite element modelling of bending of rail track

To understand the amount of the curvature bending moment affect to the longitudinal thermal stress, a finite element model was created to carry out the numerical study. In brief, the strategy of the numerical method was to create a finite element model of a 10 meter length rail (the length is same as the 10 m chord for versine measurement), with applying the side pressure on the rail, and the displacement in the middle of the 10 m rail equal to the versine (10 m chord) of a specified rail radius. Hence, the bending stress in the longitudinal direction that caused by the curvature of curved track can be obtained from the simulation. Then, the longitudinal stress caused by the bending can be calculated to equivalent rail temperature changing. By this way, the deduction of the neutral temperature that induced by the curvature bending track can be understood. The commonly-used finite element software – ANSYS was applied to carry out the numerical study.

For this case study, the versine value at the circular curve of a sharp curve which radius is equal to 300 m was calculated out. The worked out versine value is applied as the target deformation value in the x-direction on the finite element model. For this example the versine was calculated as 41.7 mm. For the devised finite element model, the rail was simulated as the rail profile of the AIS 107LB rail with a 2.86° to the horizontal direction, which is used to simulate the slope of rail seat of 1:20. The rail will be simulated as the low rail of a sharp curve. To achieve the deformation in the x-direction, the pressure load which is 6 kN/m² was applied on the rail side surface. Regarding to the boundary conditions, the rail was assumed as the side supported which is similar to a three point bending test support condition.

The x-direction deformation of the finite element analysis is 42.4 mm, very close to the designated versine value which is 41.7 mm. The deformation shape is shown in Figure 16. The most important concern is the distribution of the stress on the longitudinal direction (Z-direction) at the bottom of rail head and the neck.

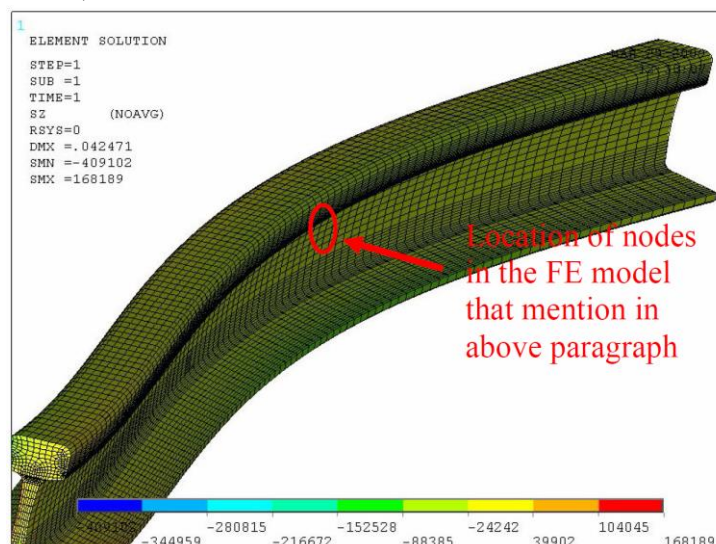


Figure 16: Z-component stress distribution and its deformation shape (scale is 10 times to the actual) of the convex rail's FE model

In addition, the detailed plot of convex side at the maximum versine value which is 42.4 mm located at the middle of the 10 meter rail model shown in Figure 16. From the finite element results, the z-direction stress at the location that has the maximum versine value was studied. At the position of the bottom of the rail head and the rail neck area (the locations to

carry out the RailScan measurement), the stress values at z-direction from the up nodes to bottom nodes are -30.258 MPa, -25.223 MPa, -20.126 MPa, -15.037 MPa, -12.103MPa, -9.9 MPa, respectively. For the CWR track 2.4 MPa stress in the longitudinal direction equal to 1 °C neutral temperature change. Hence, for the above stress values it means on the R = 300m shape curves on the low rail of the circular curve, the bending from the rail curvature can induce -4.1 to -12.6 °C neutral temperature deduction. The average value is equal to -7.82 °C.

Comparing with the sharp curve CWR module with the radius of R = 300 m (the CWR module 319.630km-319.911km), the difference between the RailScan result and cutting rail method is -7.21 °C. It is very close to the result from finite element analysis, which is -7.82 °C.

b. Finite element modelling of track strengthening

To understand the amount of influence of ambient temperature change on longitudinal stress distribution on the CWR track, a finite element model was also created to carry out the numerical study by using ANSYS again. To ensure the high accuracy of the FEA model and minimise the influence of its boundary condition, a full scale model of a 100-m curve track was created. Rail and concrete sleepers were simulated by using beam elements with the cross-section input data that are the same as its original shape profile.

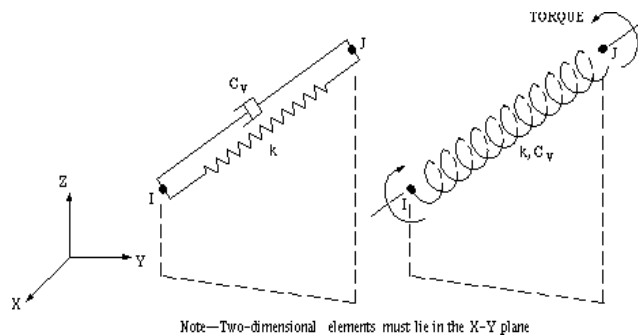


Figure 17: Combined spring-damper element (COMBIN14) used to simulate the ballast resistance on concrete sleeper, ANSYS Co., 2007.

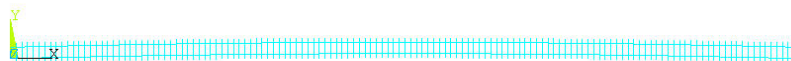


Figure 18: The FEA model which is created to simulate a 100-meter length CWR track of the Sydney – Broken Hill line

Non-linear node-to-node contact elements were applied to simulate the contact and interaction of fasteners and steel rails. The contact problems of the FEA model involve of small relative sliding between contact surfaces and the geometric nonlinearities of the whole structure. The toe load of fasteners were input as the “normal stiffness” k_N . The “sticking stiffness” k_S represents the stiffness in the tangent direction and a input data 0.22 is chosen as the coefficient of friction between the fastener and steel rail plus coefficient between steel and rubber pad.

Lateral and longitudinal resistances of ballast on each sleeper were simulated by using the combined spring-damper with different specified equivalent input stiffness values, which was modelled by using spring-damper element (COMBIN14). The torsion capability of the spring-damper element was fixed for simplification. These elements were directly connected with the beam element of concrete sleepers in the longitudinal and lateral directions.

The boundary conditions of the CWR rails were assumed to be fixed-fixed on one end and fixed in the Y direction on the other end. The spring elements that representing the ballast lateral resistance are fixed on their field side directions, which are the same as the condition of ballast where outside of concrete sleepers. For the nonlinearities of the majority materials in the FEA model, multi-liner Kinematic hardening and von Mises equivalent stress theories were followed.

The thermal load that is equal to 10 °C was applied on the end of the AIS107LB rails. From the FEA solution it can be found that the results of the longitudinal stress changing along the two rails under the thermal load is averagely equal to 9.5 °C of neutral temperature changing. This is confirmed that the average 8.2-kN low toe load of the fastener could not provide enough resistance loading to control the originally set-upped neutral temperature. And it can be seen as evidence to show the high accuracy of the RailScan system.

8. Main Research Findings

A large number of results from MBN technology based measurements and testing works in recent years have shown that the RailScan system is a sophisticated but cost effective method of providing accurate and reliable data to monitor the condition of neutral temperature and stress distribution in a railway section. It is also a very useful tool for track maintenance and research on CWR.

The stability of a specified CWR track module is highly depends on its track strengthen (i.e. condition and type of rail, sleeper, sleeper spacing, fastening systems, ballast profile, etc.). For the railway track on the Broken Hill line, on many sections, the structural strength of the CWR track are relatively low, because of the timber sleepers, fatigued steel sleepers, dog-spike fastening systems which usually cannot provide enough resistant force to control the creep of the long rail under the very harsh environment. Hence, on some track sections, the neutral temperature of the CWR track can be changing during one day from cold night to very hot noon time.

The neutral temperature at each point along a curve was found to be dependent on the curve geometry, being lower for a circular curve and higher in transition curves. From the measurements results which are represented in section 7, it was found that the neutral temperature can be higher in curve transitions than in the curve itself. The bending stress in rail installed in sharp curves can influence the thermal stress distribution in the longitudinal direction. This was shown to be related to the radius of the curve, the smaller the radius the greater the decrease in longitudinal stress.

For the track modules that installed on steep slope, the gradient can significantly impact the distribution of the longitudinal stress. From the results of in-field measurement, the bottom point of a steep slope located track module is the lowest neutral temperature point. Hence, the weakest point of a CWR track which installed on the steep slope is located at the lowest point of the slope.

Moreover, the nonlinear finite element model is a very useful tool to carry out the analysis of the CWR track at different specified locations. Some further studies will be carried out when the FEA models are further improved.

9. Acknowledgement

The authors would like to express gratitude to Mr. Ken Sherwood, the former Managing Director of Pandrol Australia Pty Ltd and Mr. Robert Rex, the Managing Director of Rex Lok Pty Ltd. for their kind help for the rail fastening system knowledge and condition analysis. Without their assistant and support this paper could not have been finished.

10. References

- Chikazumi S (1964). *Physics of magnetism*. John Wiley & Sons.
- Kerr A (2003). *Fundamentals of railway track engineering*. Simmons-Boardman Books.
- Kish A (2009). *Guidelines to best practices for heavy haul railway operations - Infrastructure construction and maintenance issues*. International Heavy Haul Associations.
- ANSYS Co. (2007). *Theory reference for ANSYS and ANSYS workbench, Release 11.0*. ANSYS Inc. and ANSYS Europe Ltd.
- Wang P and Liu X (2007). *The theory of calculation and design method of CWR track within turnout*. The Xinan Jiaotong University Publisher.

Maertens M (2018). Modelling of track stability in crossings with a finite element model. Master thesis of science in civil engineering. Department of Civil Engineering, Faculty of Engineering and Architecture, Ghent University. 2018, Ghent, Belgium.

Landuyt B (2017). Modelling of track stability in turnouts with a finite element model. Department of Civil Engineering, Faculty of Engineering and Architecture, Ghent University. 2017, Ghent, Belgium.

Zhang R and Wu H (2011). Using magnetic Barkhausen noise technology and finite element method to study the condition of continuous welded rails on the Darwin-Alice Springs line. *Journal of Civil Engineering and Architecture*, ISSN 1934-7359, USA, July 2011, Volume 5, No. 7 (Serial No. 44), 596-605.

Yang Y and Gu A (2006). Using ANSYS software to study the stability of CWR track. *Railway Engineering*. September. 2006. (in Chinese).

Zhang R, Wu H, Karsten A, Yang R & Pleasance L (2015). Better Understanding of Stability of Turnouts in CWR Track by In-Field Measurement and Numerical Study. Proceeding of 12th International Heavy Haul Conference. P337-344. 21-24 June, 2015. Perth, Australia.

Moller R, Radmann P, and Zhang R (2009). Using magnetic Barkhausen noise technology and numerical method to study the condition of continuous welded rails on Australian heavy axle track. *9th International Heavy Haul Conference*. June, 2009. Shanghai, China.

Wegner A (2004). Non-destructive determination of the stress free temperature in CWR tracks. *International Rail Forum*. Madrid. November, 2004.

Wegner A (2007). Prevention of track buckling and rail fracture by non-destructive testing of the neutral temperature in cw-rails. *8th International Heavy Haul Conference on "High Tech in Heavy Haul"*. June, 2007. Kiruna, Sweden.

Wegner A, Hofmann M, Radmann P, Zhang R, and Dubbins F (2011). Management of longitudinal rail forces by non-destructive SFT monitoring in CW Tracks. 10th International Heavy Haul Conference. June, 2011. Calgary, Canada.